Guido Gessner, Mahdi Jamili, Pascal Tomczyk, Dirk Menche, Roland Schönherr, Toshinori Hoshi and Stefan H. Heinemann*

Extracellular hemin is a reverse use-dependent gating modifier of cardiac voltage-gated Na^+ channels

https://doi.org/10.1515/hsz-2022-0194
Received June 1, 2022; accepted August 10, 2022;
published online August 29, 2022

Abstract: Heme (Fe^{2+}-protoporphyrin IX) is a well-known protein prosthetic group; however, heme and hemin (Fe^{3+}-protoporphyrin IX) are also increasingly viewed as signaling molecules. Among the signaling targets are numerous ion channels, with intracellular-facing heme-binding sites modulated by heme and hemin in the sub-μM range. Much less is known about extracellular hemin, which is expected to be more abundant, in particular after hemolytic insults. Here we show that the human cardiac voltage-gated sodium channel $hNa_V1.5$ is potently inhibited by extracellular hemin ($IC_{50} \approx 80$ nM), while heme, dimethylhemin, and protoporphyrin IX are ineffective. Hemin is selective for $hNa_V1.5$ channels: $hNa_V1.2$, $hNa_V1.4$, $hNa_V1.7$, and $hNa_V1.8$ are insensitive to 1 μM hemin. Using domain chimeras of $hNa_V1.5$ and rat $rNa_V1.2$, domain II was identified as the critical determinant. Mutation N803G in the domain II S3/S4 linker largely diminished the impact of hemin on the cardiac channel. This profile is reminiscent of the interaction of some peptide voltage-sensor toxins with Na_V channels. In line with a mechanism of select gating modifiers, the impact of hemin on $Na_V1.5$ channels is reversely use dependent, compatible with an interaction of hemin and the voltage sensor of domain II. Extracellular hemin thus has potential to modulate the cardiac function.

Keywords: heme; $Na_V1.5$; *SCN5A*; sodium channel; voltage sensor.

***Corresponding author: Stefan H. Heinemann,** Department of Biophysics, Center for Molecular Biomedicine, Friedrich Schiller University Jena and Jena University Hospital, Hans-Knöll-Straße 2, D-07745 Jena, Germany, E-mail: stefan.h.heinemann@uni-jena.de. https://orcid.org/0000-0002-4144-0251
Guido Gessner, Mahdi Jamili and Roland Schönherr, Department of Biophysics, Center for Molecular Biomedicine, Friedrich Schiller University Jena and Jena University Hospital, Hans-Knöll-Straße 2, D-07745 Jena, Germany, E-mail: guido.gessner@uni-jena.de (G. Gessner), mahdi.jamili@uni-jena.de (M. Jamili), roland.schoenherr@med.uni-jena.de (R. Schönherr)
Pascal Tomczyk and Dirk Menche, Kekulé-Institute for Organic Chemistry and Biochemistry, University of Bonn, Gerhard-Domagk-Straße 1, D-53121 Bonn, Germany, E-mail: pascal.tomczyk@uni-bonn.de (P. Tomczyk), dirk.menche@uni-bonn.de (D. Menche)
Toshinori Hoshi, Department of Physiology, University of Pennsylvania, Philadelphia, PA 19104-6085, USA, E-mail: hoshi@penmedicine.upenn.edu

Introduction

Heme (Fe^{2+}-protoporphyrin IX) is an abundant prosthetic group with key functions in redox reactions of the respective hemo-proteins (Ponka 1999; Tsiftsoglou et al. 2006). While synthesis of heme in the mitochondria and various functions in hemo-proteins are well established, the trafficking of heme within and between cells as well as the role of unbound or "labile" heme in the cytosol are subject of intensive investigation (e.g., Hanna et al. 2016). Such labile heme appears to be relevant because various so-called heme-regulated proteins are affected by the free heme level in the cytosol. For example, the transcriptional repressor of the hemeoxygenase-1 gene, BACH1, is modulated by intracellular heme at a concentration of about 100 nM (Ogawa et al. 2001).

Ion channels are among the potential target proteins of labile intracellular heme. The first example identified was the voltage- and Ca^{2+}-gated K^+ (BK_{Ca}) channel, which harbors classical heme-binding sites found in cytochromes. Heme acts as a BK_{Ca} gating modulator; heme inhibits the channel at positive voltages (Tang et al. 2003) whereas it increases the channel activity at negative voltages (Horrigan et al. 2005). Subsequently, several other ion channel types were also identified to be regulated by heme. Interaction of heme with protein segments responsible for rapid K^+ channel inactivation result in prominent gain-of-function effects (Coburger et al. 2020; Sahoo et al. 2013). Epithelial Na^+ channels (Wang et al. 2009), ATP-sensitive K^+ channels (K_{ATP}) (Burton et al. 2016), and voltage-gated K^+ channels of the ether à go-go superfamily (Burton et al. 2020; Sahoo et al. 2022) are examples where heme has a loss-of-function impact. In all these cases, the effects of

heme were similar to its oxidized form hemin (Fe^{3+}-protoporphyrin IX).

Much less is known about the potential impact of extracellular heme or hemin on effector proteins. Various extracellular proteins with hemin-binding capacity have been identified (e.g., (Wißbrock et al. 2019)), but the potential impact of extracellular heme or hemin on protein function is not clear. The binding of heme or hemin to abundant extracellular proteins such as serum albumin and hemopexin should keep the concentration of "free" heme in the extracellular space at a low level. Extracellular "labile" heme or hemin can be considered a stress factor or alarmin (Soares and Bozza 2016) and may affect various physiological processes including innate immunity (Jentho et al. 2021). Pathophysiological conditions, such as sickle cell anemia, cardiac ischemia-reperfusion, malaria, or local hemorrhage can be associated with massive release of heme/hemin from hemoglobin or myoglobin, thus overloading the extracellular heme scavenging system (Sawicki et al. 2015). In the heart, a compact organ whose function relies on the precise timing of a plethora of ion channels and transport proteins to ensure safe cardiac rhythmicity, excess extracellular hemin may have implications for their concerted action. In fact, some of the channels regulated by intracellular heme [K_{ATP} (Burton et al. 2016) and $K_V11.1$ (Sahoo et al. 2022)] are expressed in the heart. Here, we focus on extracellular hemin and address voltage-gated sodium channels (Na_V), which are responsible for the initial fast upstroke of the cardiac action potential.

Na_V channels are large membrane proteins of four homologous domains (I–IV), each organized with 6 transmembrane segments (S1-S6) with the pore loops between S5 and S6 determining the selectivity of the channel for Na^+ ions (Heinemann et al. 1992b). Nine *SCNA* genes in the human genome code for such pore-forming α-subunits ($Na_V1.1$–1.9) with different tissue distribution. $Na_V1.5$ (*SCN5A*) is primarily found in the heart, while $Na_V1.4$ is found in skeletal muscle, $Na_V1.1$, $Na_V1.2$ in the central nervous system, and $Na_V1.7$–$Na_V1.9$ in the peripheral nervous system. Although some exceptions exist, in most excitable cells the major role of Na_V channels is to initiate action potentials by permitting Na^+ influx once the cell membrane has reached a certain level of depolarization. To support rapid action potential firing while limiting cellular overexcitation, Na_V channels undergo rapid inactivation once opened. Malfunctioning of this inactivation process causes a gain-of-function and gives rise to a plethora of hereditary and acquired diseases such as myotonia, epilepsy, cardiac arrhythmia, and erythermalgia (Savio-Galimberti et al. 2012). Loss of Na_V function due to gene mutation can also lead to severe consequences as exemplified in various forms of epilepsy ($Na_V1.2$), indifference to pain ($Na_V1.7$), or Brugada syndrome ($Na_V1.5$) – a specific form of cardiac arrhythmia (Li et al. 2020). Even more prevalent is the spectrum of acute symptoms induced by low-molecular weight compounds, such as prescribed drugs or toxins affecting Na_V channels (e.g., Daimi et al. 2022; de Lera Ruiz and Kraus 2015). For such molecules, the potential impacts on Na_V channels can be classified according to the molecular mechanism of action, separating them into "pore blockers" and "gating modifiers". The former obstruct the ion permeation pathway, while the latter interfere with protein conformational changes, i.e., the voltage-dependent opening and closing of the channel complex. Mixed forms do exist, with local anesthetics serving as prominent examples: they typically block the ion permeation pathway by binding to the intracellularly-faced channel vestibule but also affect channel activation and inactivation (Körner et al. 2022).

Given the importance of Na_V channels for rapid electrical signaling, it does not come as a surprise that evolution has brought about numerous molecules that potently and specifically interfere with Na_V channels and hence are used as effective toxins for prey capture and predator defense. Among them are plant and bacterial compounds such as veratridine, tetrodotoxin (TTX), and saxitoxin (STX). STX and TTX are prototypical Na_V-channel inhibitors; they are traditionally used to discriminate Na_V channel isoforms because a single residue in the pore loop of domain I determines the TTX/STX sensitivity: toxin resistant $Na_V1.8$ and $Na_V1.9$ (serine), diminished sensitivity of $Na_V1.5$ (cysteine), and sensitivity of the remaining Na_v channels (tyrosine or phenylalanine). There is also a long list of Na_V-channel-specific peptides produced by higher organisms (Wisedchaisri and El-Din 2022). While μ-conotoxins from marine cone snails are Na_V-channel pore blockers, most of the other toxic peptides are voltage-sensor toxins that interfere with the channel's activation or inactivation. The major difference in mechanism among the voltage-sensor toxins resides in which of the four voltage sensors is affected by the toxin [e.g., scorpion β-toxin and μO-conotoxins affect the voltage sensor in domain II; scorpion α-toxins and δ-conotoxins affect the voltage sensor in domain IV (Heinemann and Leipold 2007)].

Here we identified cardiac $Na_V1.5$ channels as specific targets of extracellular hemin. Functional analysis of various Na_V isoforms, chimeras and point mutants revealed that hemin exerts an inhibitory influence on $Na_V1.5$ channels with a half-inhibitory concentration of 80 nM. Hemin does not act as a pore blocker but rather works like a voltage-sensor toxin. Similar to μO-conotoxins, the effect of hemin on the channel is strongly use or state dependent, with channel activation diminishing the hemin effect. The

molecular determinant underlying the mechanism of channel modulation resides in the voltage sensor of domain II with a single amino-acid position (N803), which is unique to $Na_V1.5$, rendering cardiac Na_V channels particularly sensitive to extracellular hemin. These results suggest physiological or pathophysiological roles of extracellular hemin in cardiac function.

Results

Hemin inhibits $Na_V1.5$ channels

Cardiac voltage-gated sodium channels ($Na_V1.5$) are of prime importance for the generation of cardiac action potentials, and gain-of-function as well as loss-of-function mutations of the corresponding *SCN5A* gene typically lead to severe cardiac arrhythmia. To infer the potential impact of extracellular hemin, such as that resulting during acute hemolysis, on $Na_V1.5$ channels, we expressed *SCN5A* in HEK293T cells and studied the influence of extracellularly applied hemin while recording depolarization-activated currents in the whole-cell mode of the patch-clamp method. As shown in Figure 1A and B, the peak inward current elicited with depolarizations to −30 mV was rapidly (<1 min) and potently (by 90 ± 4%, n = 7) diminished by application of 2 µM hemin (for voltage dependence see below). This effect was only slowly reversible on washout of hemin, after about 30 min reaching a relative current amplitude of 48 ± 8% of the control value before hemin application (Figure 1A–C). Similar experiments performed with various concentrations of hemin resulted in concentration-dependent current inhibition following a binding curve described with the Hill equation (Eq. (5)). The apparent half-inhibitory constant (IC_{50}) was 81 ± 15 nM and the Hill coefficient was 0.68 ± 0.07 (Figure 1D and E), suggesting that about one hemin molecule might be sufficient to exert its effect on the channel.

These experiments showed that $Na_V1.5$ channels are about as sensitive to extracellular hemin as other ion channels have been reported to be sensitive to intracellular heme or hemin (see Introduction). This sensitivity is remarkable because the extracellular hemin concentration can reach much higher levels than reported for the cytosol, although the extent of free or labile hemin in the extracellular space is not yet clearly established (Soares and Bozza 2016).

Specificity for hemin over heme

To evaluate the chemical structural specificity of hemin in inhibiting $Na_V1.5$ channels, we compared the influence

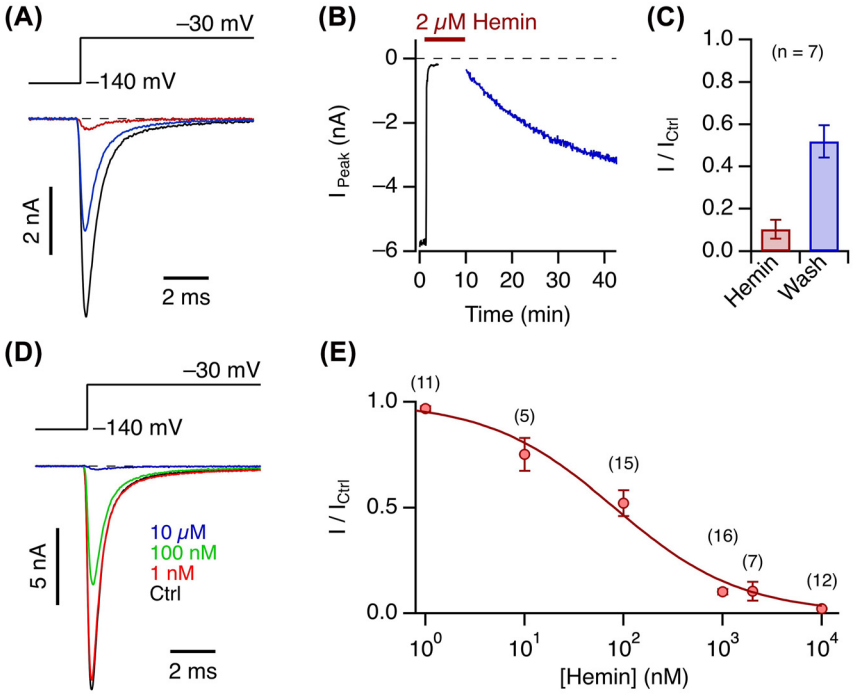

Figure 1: Hemin-induced $Na_V1.5$ current inhibition and reversibility.
(A) Whole-cell currents according to the indicated pulse protocol before (black) and after application of 2 µM hemin (brown), as well as about 30 min after wash-out of the hemin (blue). (B) Time course of peak currents from the experiment shown in (A) with the indicated period of hemin application. The data points shown in blue were recorded after washout of hemin. (C) Mean remaining peak current with respect to the control in the presence of 2 µM hemin and about 30 min after washout. (D) Whole-cell currents according to the indicated pulse protocol before (black) and after application of hemin at the indicated concentrations (color). (E) Concentration dependence of hemin-induced peak current inhibition at −30 mV. The superimposed curve is the result of a Hill fit (Eq. (5)) yielding an IC_{50} of 81 ± 15 nM and a Hill coefficient of 0.68 ± 0.07, reaching full inhibition at high concentration. Error bars in (C) and (E) are sem values with n in parentheses.

of hemin with protoporphyrin IX (PpIX), i.e., the scaffold of hemin without the central metal ion, and heme (Fe^{2+}-protoporphyrin IX, reduced with DTT), each applied at 1 µM. In both cases the impact on the peak current at −30 mV did not exceed 10%, even after exposure for 5 min (Figure 2); the central Fe^{3+} is thus essential. We also tested 1 µM dimethylhemin (dMH), i.e., hemin in which methyl ester groups replace the carboxylate groups of the protoporphyrin scaffold, and found no discernible impact on the current amplitude (Figure 2). These results taken together indicate that a protoporphyrin ring with carboxylate groups and the central Fe^{3+} ion are required. Because of the strong hydrophobicity, PpIX and dMH were from stock solutions in DMSO, while hemin was typically pre-dissolved in NaOH. We therefore confirmed that hemin from a DMSO-based stock solution has the same impact on the channel as hemin from NaOH (Figure 2). Close inspection of the time course of hemin-induced current inhibition (Figure 2C) furthermore showed that the effect of hemin on the channel develops in two phases: a major fast one – with a time constant of about 5 s, largely limited by the speed of hemin application and mixing – and a slow component with a time constant on the order of 110 s. The existence of such two phases may indicate two distinct mechanisms of channel inhibition or multiple allosterically coupled processes leading to channel inhibition.

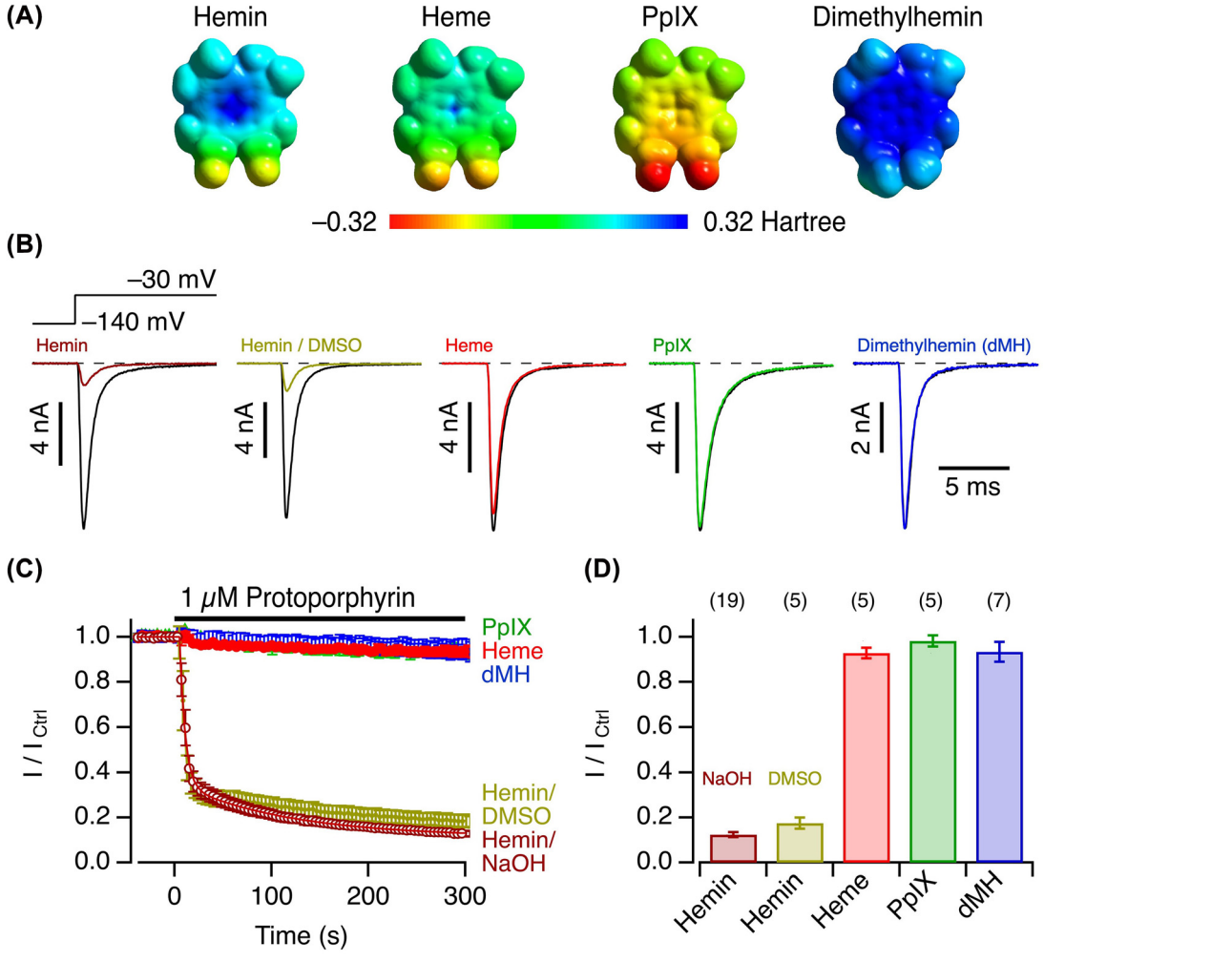

Figure 2: Impact of hemin and related compounds.
(A) Electrostatic surface potentials of hemin, heme, PpIX, and dimethylhemin (dMH). (B) Whole-cell currents according to the indicated pulse protocol before (black) and about 5 min after application of hemin (from NaOH and DMSO stock solutions), PpIX (DMSO), heme (NaOH), or dMH (DMSO) at 1 µM (color). (C) Mean time course of peak currents at −30 mV, recorded at intervals of 4 s, with the indicated application of 1 µM PpIX, heme, dMH, hemin from NaOH stock solutions (open circles), or from DMSO stock solutions (filled circles). The curve superimposed to the hemin/NaOH data is the result of a double-exponential fit yielding a fast time constant of 5.7 ± 0.2 s, a slow time constant of 113 ± 7 s, a relative contribution of the fast component of 73.7 ± 0.4%, and a saturating level of current inhibition at 11.3 ± 0.3% of the control values before hemin application. (D) Mean remaining current after 5 min application of the indicated compounds at 1 µM. Data in (C) and (D) are means ± sem with *n* in parentheses (D).

The different impacts of hemin and heme make $hNa_V1.5$ channels potential real-time sensors for monitoring the oxidation or reduction of the central iron ion under physiological conditions. As shown in Supplementary Figure 1, 5 min preincubation of hemin with 1 mM DTT eliminates its potency to inhibit $hNa_V1.5$ channels. When hemin and DTT were mixed only about 10 s before application to the cell, the initial current inhibition is followed by a slow relief, thus unmasking the kinetics of hemin reduction to heme with the consequence of losing its ability to inhibit $Na_V1.5$-mediated currents.

The markedly contrasting impact of hemin and heme, only differing in the oxidation state of the central iron ion, may suggest that the mechanism of inhibition involves an oxidation process. In this respect an obvious candidate feature of cardiac Na_V channels is a unique cysteine residue in the extracellular pore region of domain I (Heinemann et al. 1992a), a site also known to be the major determinant for the sensitivity of Na_V channels towards the inhibitors TTX and STX (Terlau et al. 1991). We therefore examined a variant of $hNa_V1.5$ in which a tyrosine replaces the aforementioned cysteine residue: C373Y. As shown in Supplementary Figure 2, $Na_V1.5$-C373Y responds to hemin in a similar manner to the $hNa_V1.5$ wild type, thus rejecting the idea that hemin specifically modifies C373, giving rise to the observed decrease in current amplitude.

Mechanism of channel inhibition

The strong impact of hemin on $Na_V1.5$-mediated Na^+ currents thus far was characterized using depolarizations to −30 mV, a voltage that does not fully activate all channels. To assess a potential voltage dependence of the hemin action, we measured channel activation and inactivation at different voltages under control conditions and after application of hemin at a concentration slightly above the experimentally determined IC_{50} value to retain enough current for faithful analysis (100 nM). As shown in Figure 3A and B, hemin diminished the peak current amplitude at all examined voltages in a similar manner. Moreover, the parameters describing voltage-dependent channel activation (V_m and k_m) were not noticeably altered. Superposition of scaled traces at various voltages furthermore shows that the kinetics of channel activation and inactivation are not markedly affected (Figure 3C).

Because it is conceivable that hemin acts as a fast and partial channel blocker, effectively decreasing the single-channel current amplitude, we also performed non-stationary noise analysis of repetitive current measurements at 3 different voltages (−50, −30, −10 mV). In experiments with 1 μM hemin application, thus leaving only about 15% of the initial current, the single-channel conductance estimates before and after hemin application were identical within the error limit (Figure 3D and E). We can therefore exclude rapid pore blocking as a mechanism responsible for the current size reduction.

Voltage dependence of fast inactivation was only marginally affected, shifting the half-maximal inactivation voltage from −101.9 ± 2.1 mV for control to −108.6 ± 3.0 mV in the presence of 100 nM hemin (Figure 3F and G). This slight left-shift may indicate a minor influence of channel inactivation favored in the presence of hemin and may therefore suggest that the repetitive depolarizations applied in our assays (Figures 1B and 2B) may progressively drive a greater fraction of the channels into an inactivated state. We therefore compared hemin-application experiments in which we repetitively depolarized the cells every 4 s with an alternative protocol in which depolarizations were paused immediately after hemin application and resumed 1 min later. As shown in Supplementary Figure 3, the relative peak current after this pause had the same amplitude as currents measured under continuous pulsing conditions, thus excluding a marked use dependence for a pulse-repetition interval of 4 s (0.25 Hz). Stated in a different way, the inhibitory impact does not require depolarization to open the channels.

Numerous low-molecular weight compounds, such as local anesthetics, have the propensity of blocking Na_V channels in a strongly use- or state-dependent manner, enhancing channel block when the channel is open. Such use dependence is typically observed during a train of action potentials, and it may only become visible at much higher rates of pulse repetition than the pulse frequency of 0.25 Hz examined above. We thus measured the impact of hemin on $hNa_V1.5$ channels with trains of depolarizations to −10 mV at frequencies of 2, 5, 10, 20, and 50 Hz. While under control conditions some current reduction during the train due to cumulative inactivation becomes apparent at 10 Hz and above, the situation is quite the opposite in the presence of hemin (Supplementary Figure 4). As illustrated for a recording protocol with 20 Hz pulse frequency, hemin-induced current inhibition becomes *smaller*, rendering the currents progressively greater in size, within the train of pulses (Figure 4A): *reverse* use dependence. Comparison of various pulse frequencies (Figure 4B) reveals that recovery from hemin-induced current block is augmented with increasing pulse frequency. Even at the lowest examined frequency of 2 Hz, clear reverse use dependence is observed.

In the results shown in Figure 4A, the relief from channel inhibition by hemin was elicited by repetitive

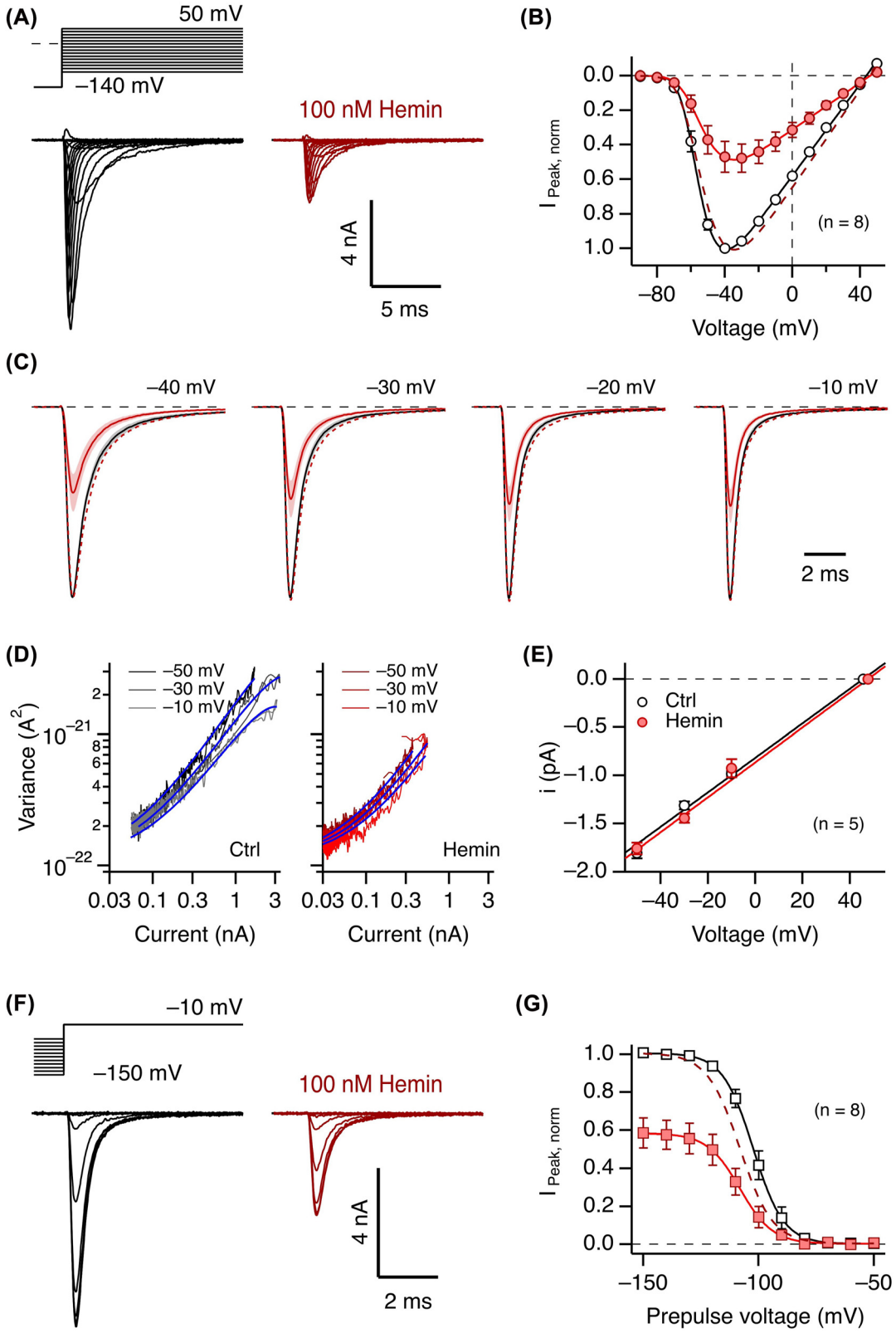

Figure 3: Voltage dependence of activation and inactivation.
(A) Representative whole-cell $hNa_V1.5$ channel currents measured according to the indicated pulse protocol before (black) and about 5 min after application of 100 nM hemin. (B) Mean peak currents (±sem), normalized to the control values at −40 mV before (open circles) and after (filled circles) application of 100 nM hemin. The continuous lines are fits according to Eq. (1); the dashed line is the fit to the data with hemin, scaled by a factor of 2.07 to match the amplitude of the control. Control: V_m = −64.3 ± 1.1 mV, k_m = 6.9 ± 0.5 mV; 100 nM hemin:

5 ms pulses to –10 mV. To infer the time and voltage dependence, two-pulse recording protocols were devised to vary both time and voltage parameters independently. As depicted in Figure 4C and D, the voltage dependence of a 50 ms prepulse exhibits a half-maximal unblock voltage of about –32 mV and a slope factor of 21 mV. Such prepulses had no effect on $hNa_V1.5$ currents in the absence of hemin (Figure 4D, open symbols). Likewise, variations of the length of a prepulse to –10 mV indicates saturation at about 100 ms and a time constant of 32 ms (Figure 4E and F). The experiment shown in Figure 4G and H determines the kinetics of reestablishing the hemin effect at –140 mV after current inhibition was partially removed with a 50 ms/40 mV prepulse. Under this condition, the resulting average time constant was 210 ms, thus indicating a comparatively slow return to the hemin-inhibited channel state. Based on these estimates of voltage- and time-dependent hemin action, a prepulse to 40 mV for 50 ms – a pulse causing less depolarization than occurring during a human cardiac action potential – effectively removes a large fraction of the hemin effect on the channel. Current-voltage relationships, recorded without and with such a prepulse, clearly demonstrate the strong state dependence of the hemin impact on $Na_V1.5$ channels (Supplementary Figure 5).

The impact of hemin on $Na_V1.5$ is specific for the channel type

The strong reverse use dependence by which hemin affects $hNa_V1.5$ channels resembles the impact of so-called μO-conotoxins from marine cone snails. Such peptides of about 30 residues also inhibit Na_V channels with a pronounced reverse use dependence (Leipold et al. 2007; Zorn et al. 2006). Furthermore, scorpion β-toxins, peptides of about 60–70 residues, also suppress channel activity in a use-dependent manner (Leipold et al. 2006; Leipold et al. 2012). In both cases, the effects on Na_V channels strongly varies among different Na_V isoforms. We therefore examined the impact of 1 μM extracellular hemin on various human Na_V isoforms after expression in HEK293T cells. Neither the central nervous system channel $hNa_V1.2$, the skeletal muscle channel $hNa_V1.4$, nor $hNa_V1.7$, which is predominantly expressed in the peripheral nervous system, was noticeably affected by hemin (Figure 5). Since the TTX-resistant $Na_V1.8$ channel from the peripheral nervous system does not sufficiently express in HEK293T cells, we utilized a chimera harboring the C terminus from $rNa_V1.4$ ($hNa_V1.8c4$). Current at –30 mV of this variant was only marginally inhibited by 1 μM hemin. Thus, among the Na_V channel types examined, the cardiac isoform $hNa_V1.5$ is uniquely sensitive to extracellularly applied hemin.

Channel chimeric approach identifies the voltage sensor II as potential interaction target

The clear subtype specificity of hemin, e.g., effective on $Na_V1.5$ and ineffective on $Na_V1.2$, suggests that $hNa_V1.5$ possesses a gating mechanism more readily altered by hemin than those of other Na_V channels. As a step towards identification of the molecular locus within $hNa_V1.5$ critical for hemin's inhibitory influence, we generated domain chimeras by combining $hNa_V1.5$ ("5555") and rat (r) $rNa_V1.2$ ("2222") α-subunits to yield chimeric channels "2552", "5525", and "5255", where each number denotes the domain identification: $hNa_V1.5$ versus $rNa_V1.2$. Upon expression in HEK293T cells and examination with respect to 1 μM hemin, the rat paralog $rNa_V1.2$ is as insensitive towards hemin (Figure 6) as the human one (Figure 5). The chimeras "2552" and "5525" are still sensitive to hemin, which inhibits their current almost as much as for $hNa_V1.5$. In contrast, chimera "5255" is as insensitive to hemin as $rNa_V1.2$. Therefore, domain II appears to be of prime importance for the impact of hemin on $hNa_V1.5$. This property is also reminiscent of the effects of μO-conotoxins (Leipold et al. 2007) and of scorpion β-toxin on Na_V channels (Leipold et al. 2006; Leipold et al. 2012). With these toxins, the marked use-dependent inhibition was strongly affected by altering a single residue in the S3/S4 linker of Na_V domain II (Leipold et al. 2007; Leipold et al. 2012). This residue – N803 according to the numbering of $hNa_V1.5$ – is

$V_m = -62.7 \pm 1.3$ mV, $k_m = 9.9 \pm 0.9$ mV. (C) Superimposed mean current traces, scaled to the peak, before (black) and after (color) application of 100 nM hemin for the indicated voltages. The traces are mean values, sem indicated in shading, $n = 7$. The dashed traces are currents in the presence of hemin scaled to the peak of the control current. (D) Representative example of mean ensemble variance versus mean current without (left, black) and with 1 μM hemin (right, red) for the indicated voltage. The superimposed blue curves are the result of a global fit to all data according to Eq. (3) with the background variance and the total number of channels being identical for all. (E) Estimation of the single-channel conductance based on single-channel current amplitudes derived with nonstationary noise analysis (as in panel D) and the reversal potentials determined from the current data: control, 17.9 ± 0.3 pS; hemin, 18.1 ± 0.4 pS. (F) As in (A) for a pulse protocol with 920 ms prepulses to various voltages to assess the voltage dependence of fast inactivation. (G) Mean normalized peak currents with superimposed fits according to Eq. (2). The dashed curve corresponds to the fit to the hemin data, scaled by a factor of 1.72. Control: $V_h = -101.9 \pm 2.1$ mV, $k_h = 5.7 \pm 0.2$ mV; 100 nM hemin: $V_h = -108.6 \pm 3.0$ mV, $k_h = 6.0 \pm 0.4$ mV.

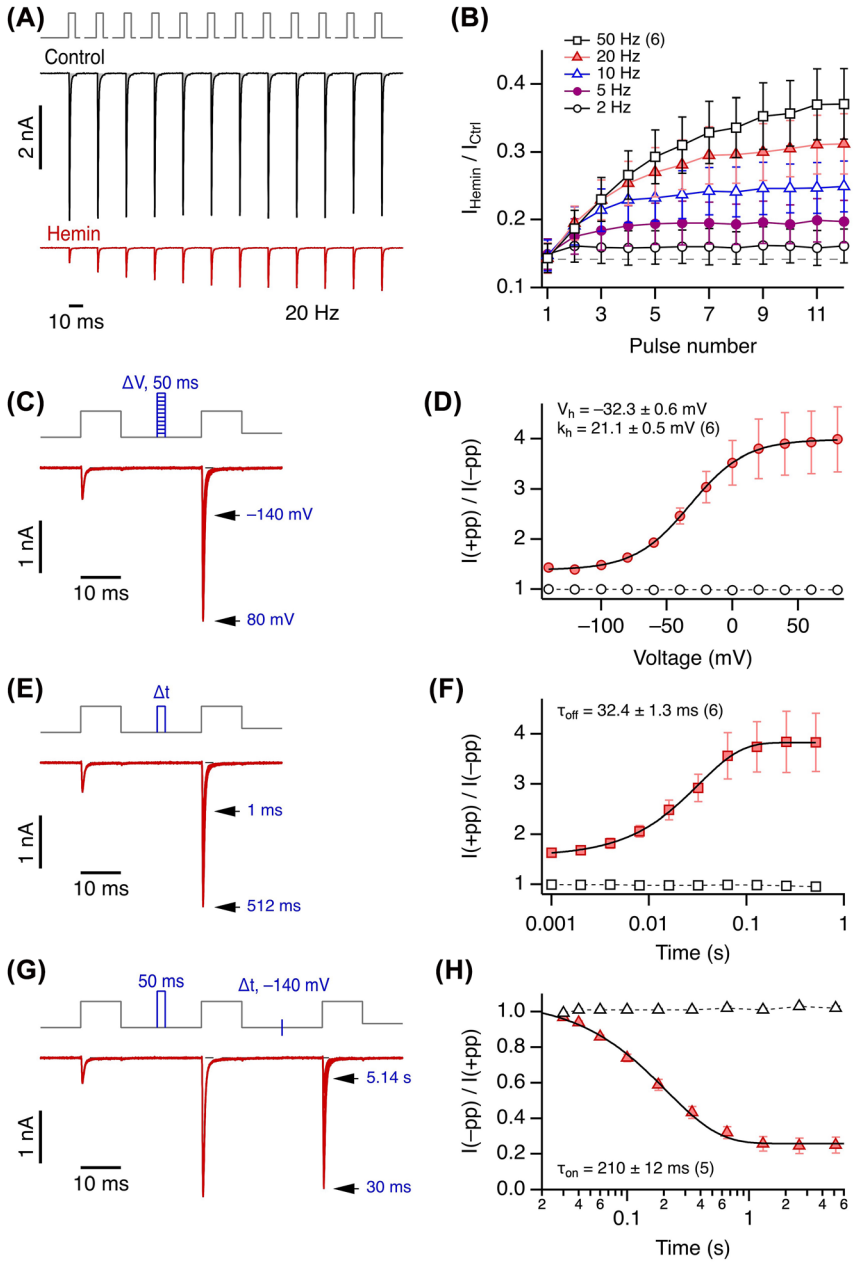

Figure 4: Reverse use dependence of $Na_V1.5$ current inhibition.
(A) *Top*, pulse protocol for measuring the use dependence of hemin action; holding potential was –120 mV. Repetitive depolarizations, 5 ms each in duration, from –120 to –10 mV were applied. The gaps indicate waiting intervals at –120 mV to yield various pulse frequencies, in this case 20 Hz. *Center* and *bottom*, whole-cell current responses of $Na_V1.5$ channels before (black) and after application of 1 µM hemin (red). (B) Mean relative change in peak current amplitude with hemin with respect to the corresponding pulse under control conditions as a function of the pulse number for the indicated pulse frequencies. Straight lines connect the data points for clarity. (C) Pulse protocol and superimposed current traces in the presence of hemin. Between the two test pulses to –10 mV to measure current, 50 ms depolarizing pulses of variable voltage followed by 40 ms at –140 mV were inserted (blue). (D) Mean relative peak current of pulse 2 over pulse 1 as a function of the prepulse voltage. Superimposed fit: Boltzmann function with the indicated parameters. Open symbols denote control values in the absence of hemin, connected by straight dashed lines. (E) Pulse protocol and superimposed current trace in the presence of hemin. Between the two test pulses, a depolarization to –10 mV of variable duration was inserted, followed by 40 ms at –140 mV (blue). (F) Mean relative peak current of pulse 2 over pulse 1 as a function of the prepulse duration. Superimposed fit: Exponential, yielding the indicated time constant. (G) Pulse protocol and superimposed current trace in the presence of hemin. Between the first and the second pulse a 50 ms depolarization to 40 mV was inserted (blue), between test pulses 2 and 3 the duration at –140 mV was varied (blue mark). (H) Mean relative peak current of pulse 3 over pulse 2 as a function of the recovery duration. Superimposed fit: Exponential, yielding the indicated time constant. Data in (B), (D), (F), (H) are mean ± sem with *n* in parentheses.

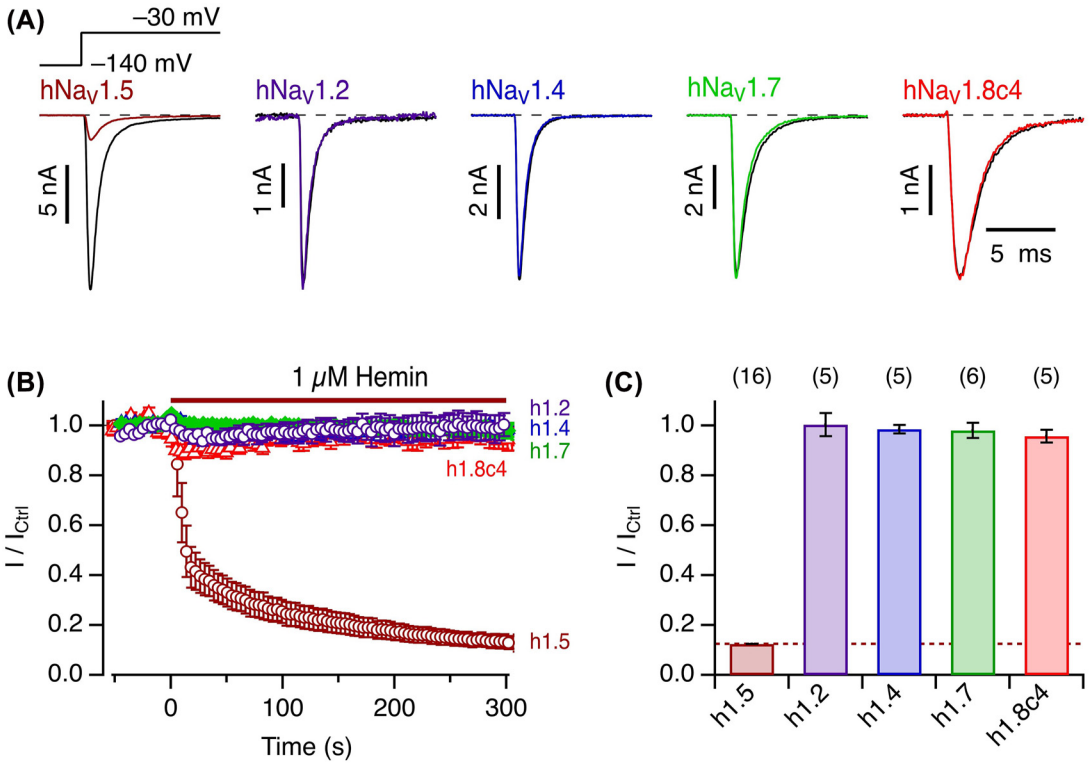

Figure 5: Specificity for cardiac $hNa_V1.5$ channels.
(A) Representative whole-cell currents according to the indicated pulse protocol before (black) and about 5 min after application of 1 μM hemin (color) for $hNa_V1.5$, $hNa_V1.2$, $hNa_V1.4$, $hNa_V1.7$, and $hNa_V1.8c4$. (B) Mean time course of peak currents at –30 mV, recorded at intervals of 4 s, for the different channel isoforms as indicated by the colors as in (A). (C) Statistics for the mean remaining current after 5 min exposure to 1 μM hemin. Data in (B) and (C) are mean ± sem with *n* in parentheses (C).

an asparagine only in $Na_V1.5$ channels while being glycine in most of the other isoforms. $hNa_V1.8$ is another exception as it harbors a serine residue at the equivalent site (Supplementary Figure 6). We thus examined variant $hNa_V1.5$-N803G and found that the impact of hemin was largely eliminated (Figure 6). The rapid current inhibition was totally absent, and even after 5 min application time the current amplitude became smaller only by about 15%. In the presence of hemin, no use dependence was observed for mutant N803G (Supplementary Figure 7).

Discussion

Intracellular hemin or heme affects ion channels by increasing or decreasing the channel activity, and various types of heme or hemin binding sites in intracellularly located protein domains have been identified (Burton et al. 2016; Burton et al. 2020; Coburger et al. 2020; Sahoo et al. 2013; Sahoo et al. 2022; Tang et al. 2003; Wang et al. 2009). Accordingly, intracellular heme and/or hemin have been suggested to act as non-genomic channel regulators. While some ion channels are particularly sensitive to hemin, such as $K_V10.1$ channels being half-maximally inhibited by low nanomolar concentrations of heme and hemin (Sahoo et al. 2022), it remains unclear under which conditions intracellular heme and/or hemin modulate ion channel function.

Here we found that the voltage-gated sodium channel $hNa_V1.5$, which is essential for generating cardiac action potentials, is potently inhibited by extracellular hemin with an IC_{50} of about 80 nM. Although extracellular hemin is efficiently scavenged by binding to serum albumin and hemopexin, marked variations in the extracellular pool of free hemin are likely to occur; pathophysiological conditions such as hemolysis, sickle-cell disease, malaria, local bleeding, and trauma may increase the hemin pool whereas anemia may decrease the pool (Roumenina et al. 2016; Sawicki et al. 2015).

Cardiac $hNa_V1.5$ channels were sensitive to extracellular hemin at ≈100 nM whereas Na_V channels from the skeletal muscle ($Na_V1.4$) or neuronal sodium channels ($Na_V1.2$, $Na_V1.7$, $Na_V1.8$) were insensitive to even 1 μM hemin (Figure 5). The unique hemin sensitivity of $hNa_V1.5$ suggests that the heart function may be subject to inhibitory modulation by extracellular hemin. Complete $Na_V1.5$

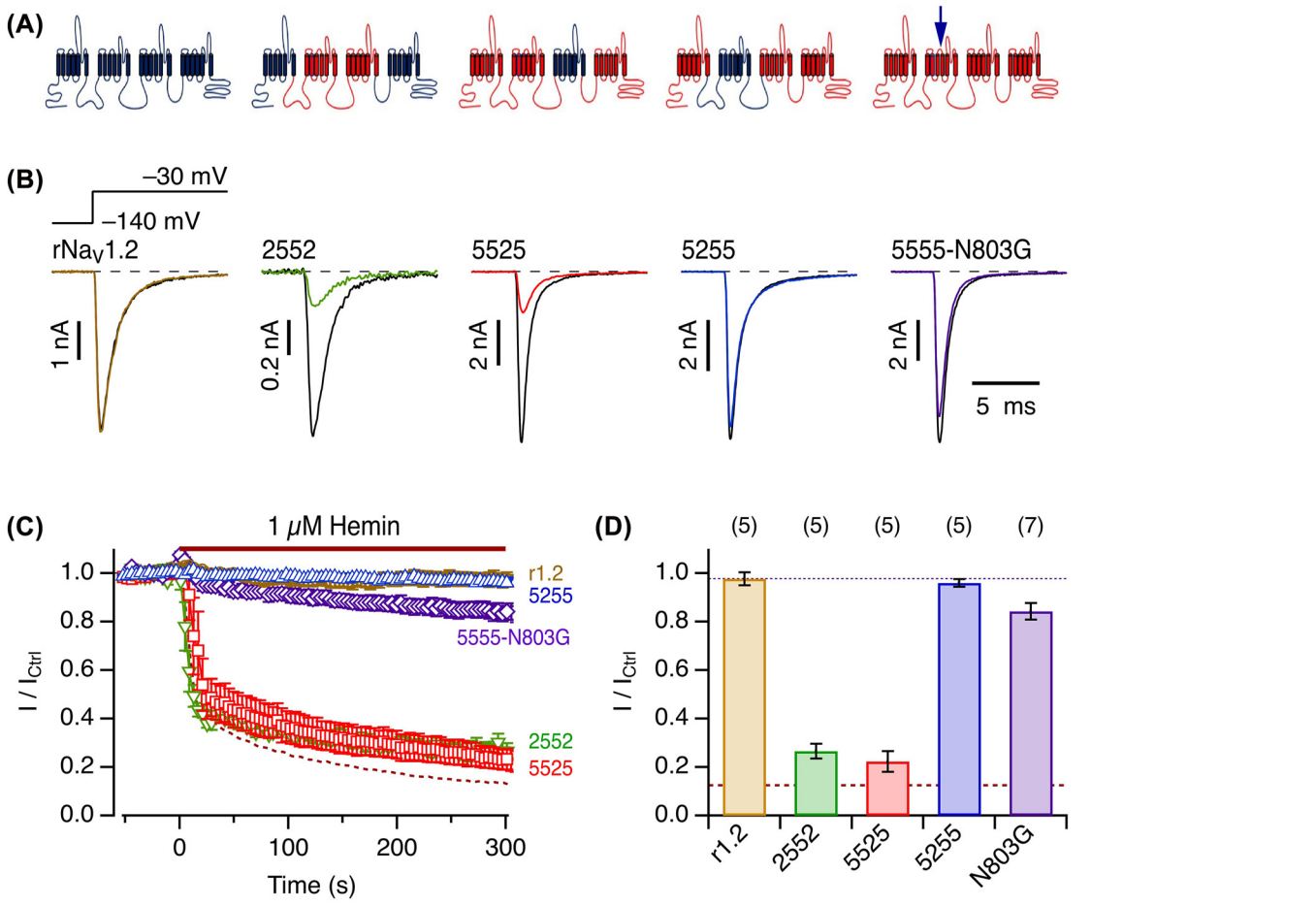

Figure 6: Molecular determinants in the voltage sensor of domain II.
(A) Cartoons of channel protein topology to illustrate the construction of domain chimeras between $rNa_V1.2$ (blue) and $hNa_V1.5$ (red). The arrow on the right marks the approximate position of residue N803. (B) Representative whole-cell currents according to the indicated pulse protocol before (black) and about 5 min after application of 1 μM hemin (color) for $rNa_V1.2$ and domain chimeras originating from $hNa_V1.5$ ("5") and $rNa_V1.2$ ("2"), 2552, 5525, and 5255, as well as the point mutant $hNa_V1.5$-N803G. (C) Mean time course of peak currents at –30 mV, recorded at intervals of 4 s, for the indicated channel isoforms. The dashed curve is the mean for $hNa_V1.5$ from Figure 5B. The colors are as in (B). (D) Statistics for the mean remaining current after 5 min exposure to 1 μM hemin. The brown dashed line marks the mean for $hNa_V1.5$ and the dotted black line the mean of $rNa_V1.2$. Data in (C) and (D) are means ± sem with *n* in parentheses (D).

inhibition is lethal because of its pivotal role in generating cardiac action potentials and partial inhibition of $Na_V1.5$ may be a predisposing factor potentially leading to diminished myocardium contractility or cardiac arrhythmia, possibly in a similar manner as *SCN5A* loss-of-function mutations leading to various forms of the Brugada syndrome (Li et al. 2020). Thus, excess extracellular free hemin may need to be considered as an additional risk factor of the cardiac disorder. In fact, cardiac problems in patients suffering from hemolytic malaria have been documented although it is unclear whether the related symptoms are caused by excess hemin, fever, or anti-malaria medication (Cader et al. 2018; Crespo et al. 2009; Meggiolaro et al. 2013; Sawicki et al.2015).

One may also consider the possibility that basal hemin and its tight association with the channel constitutes a physiological condition. This hypothesis finds support in the strong reverse use dependence that we found for the hemin–channel interaction. At concentrations less than 1 μM, hemin can substantially inhibit $Na_V1.5$-mediated Na^+ influx; however, the inhibitory influence is almost completely eliminated when the channel is activated after long-lasting depolarizations. These inhibitory characteristics suggest that during the course of a human ventricular action potential the impact of hemin should be diminished and the Na^+ influx should *increase*. This reverse use dependence of hemin-induced inhibition may provide the heart with an extra safety margin by

automatically augmenting the Na^+ current amplitude when the heart rate is suddenly increased. The possibility that hemin plays both physiological and pathophysiological roles exists, and studies on human $Na_V1.5$ channels at body temperature and exploring the full voltage and dynamic range of human action potentials may provide deeper insight.

While the potential implication of the hemin–$Na_V1.5$ interaction for cardiac function awaits detailed investigations at the cellular, organ, and organism level, the interaction is particularly interesting from the mechanistic point of view. It is not only the first case of a strong and specific influence of extracellular hemin on an ion channel protein but also is unusual in the specificity of hemin over heme. Furthermore, there is this remarkable specificity for cardiac Na_V channels. The strong impact of hemin on $hNa_V1.5$-mediated Na^+ currents cannot be accounted for by a rapid pore-blocking mechanism because the single-channel conductance was not affected by hemin. In addition, kinetics and voltage dependence of activation and inactivation were not markedly altered. Instead, hemin appears to act as a gating modifier affecting some conformational changes of the protein complex leading to voltage-dependent channel opening. This notion is firmly supported by the observed use or state dependence of the hemin effect; the functional impact of hemin depends on the channel state or its prior "use". Starting from strong channel inhibition in a resting configuration at –120 mV, the inhibitory influence is greatly diminished by depolarization or, in other words, by conformational changes of the channel protein induced by depolarization. The analysis shown in Figure 4 reveals a mid-potential for this process of about –30 mV and a voltage dependence equivalent to about 1 electron charge translocated across the membrane electric field. A time constant at –10 mV of 32 ms shows that this process is much slower than channel activation and inactivation. The biophysical analysis together (Figure 4) suggests that the reverse use dependence occurs in the physiological voltage and time ranges.

The reverse use dependence of the inhibitory impact of hemin on $hNa_v1.5$ resembles that of several peptide toxins affecting Na_V channels in a similar manner. μO-conotoxins from marine cone snails– peptides with 3 disulfide bridges – inhibit select Na_V channels similar to hemin in that their inhibitory influence is strongly diminished when the voltage sensors are preactivated with a depolarizing pulse (Leipold et al. 2007; Zorn et al. 2006). Comparison of channel isoforms and domain-wise chimeras between sensitive and insensitive channels revealed that μO-conotoxins (Leipold et al. 2007) but also scorpion β-toxins (Leipold et al. 2012) interfere with the operation of the voltage sensor in domain II. We followed the same approach here utilizing the marked functional differences of $hNa_V1.5$ (sensitive) and $rNa_V1.2$ (insensitive) channels, and showed that domain II is also a crucial determinant for the functional impact of hemin on $hNa_V1.5$ channels. Moreover, a single-site mutation at the S3/S4 linker of domain II (N803G) strongly diminished the hemin effect, suggesting that hemin interferes with the conformation change of the domain-II voltage sensor when the membrane voltage changes.

Only hemin is functionally effective on $hNa_V1.5$ among the four protoporphyrins examined (Figure 2). Structurally the four protoporphyrins differ considerably in their electrostatic potential distributions (Figure 2A). Comparison of the overall functional and the electrostatic potential characteristics suggests that both the negative carboxylate groups (hemin versus dMH) and the electropositive character at the center of the porphyrin ring (e.g., hemin versus heme versus PpIX) are important determinants of the hemin potency on $hNa_V1.5$. Additional clues about the potential roles of the negative carboxylate groups and the electropositive center of hemin are provided by the reverse use dependence feature of the inhibitory impact of hemin on $hNa_V1.5$. Opening of $hNa_V1.5$, as in many other canonical voltage-gated channels, involves movements of its S4 voltage sensors with multiple positively charged residues from the resting state to the activated state, the latter of which is stabilized in part by the electrostatic interactions between the S4 positive charges and select negatively charged residues in the extracellular sides of S1, S2, and S3 (Tao et al. 2010). These negative counter charges interact with water and ions when the voltage sensors are in the resting state at negative voltages. It is easy to speculate that the electropositive center of hemin interacts preferentially with one or more of the negative counter charges, preventing activation of the voltage sensor and thus channel opening. With strong and/or repeated depolarizations, the S4 voltage sensor displaces the hemin away from the negative counter charges. This competition for the negative counter charges between the S4 positive charges and the electropositive center of hemin may account for the reverse use dependence. It is probable that the carboxylate groups of hemin act to stabilize the molecule near the voltage sensor. Earlier studies suggested that μO-conotoxins and scorpion β-toxins, which also show reverse use dependence, are stabilized near the domain II voltage sensor in the pore loops of domain III (Leipold et al. 2006, Zorn et al. 2006). Hemin may be stabilized in a

similar manner; the pore loop of domain III does contain multiple positively charged arginine and lysine residues. Our working model based on the $hNa_V1.5$ structure (Li et al. 2021) is depicted in Supplementary Figure 8. A hemin molecule is placed between the domain-II S3 negative counter charges and the domain-III pore loop. The electrostatic interaction between the electropositive center of hemin and the negative counter charges inhibits the domain-II voltage sensor activation, contributing to the efficacy aspect of the hemin inhibitory action. In contrast, the carboxylate groups of hemin interact with the positively charged residues in the domain-III pore loop, in part contributing to the affinity aspect. According to this working model, heme and PpIX are ineffective because they lack the center electropositivity to interact with the negative counter charges. Dimethylhemin lacks the negative carboxylate groups and its stable positioning near the voltage sensor domain is severely compromised (Figure 2A). This mechanism implies that one hemin molecule might be sufficient to affect the voltage sensor in domain II. While this notion is compatible with the experimentally determined Hill coefficient being close to one, we cannot exclude that $Na_V1.5$ harbors several binding sites for hemin, possibly with lower affinity. The latter might be responsible for the slow component of current reduction following hemin application.

While only hemin inhibits $Na_v1.5$, the actual binding of hemin to Na_V channels may not differ substantially among different isoforms because some of the positively charged residues in the domain-III pore loop are conserved (e.g., K1359). Therefore, the unique phenotype of $hNa_V1.5$ channels may largely be explained by its particular structure of the domain-II voltage sensor. With the strong impact of mutation $hNa_V1.5$-N803G it is likely that this residue has a significant impact on how hemin affects the mobility of the voltage sensor. As shown in Supplementary Figure 6, most of the other Na_V channels harbor a glycine at the equivalent position. $hNa_V1.8$ is an exception with a serine residue, but N-terminal to this serine residue there is also a glycine in $hNa_V1.8$, possibly explaining the very weak impact of hemin on $hNa_V1.8c4$ (Figure 5).

Although the above hypothesis appears plausible, a potential influence of the redox property of hemin is not unambiguously excluded because heme cannot be applied under oxidizing conditions without changing its redox state. We experimentally eliminated the possibility that cysteine 373 in the pore region of domain I, which is unique for cardiac Na_V channels, plays an important role because $hNa_V1.5$-C373Y is affected by hemin in the same way as the wild type (Supplementary Figure 2). Electrophysiological recordings with hemin preincubated with DTT for different durations (Supplementary Figure 1) are in line with DTT reducing hemin to heme rather than reducing the channel protein. The possibility that the hemin impact on $Na_V1.5$ channels occurs only when some extracellular-facing segments of the protein is exposed to an oxidizing milieu, as expected under physiological conditions, remains.

Conclusions

The activity of the cardiac voltage-gated sodium channels $hNa_V1.5$ is potently and specifically inhibited by extracellular hemin whereas heme and dimethylhemin are ineffective. While a binding site for hemin at the channel protein is yet to be defined, hemin acts as a gating modifier by affecting the channel's voltage sensor in domain II. It is expected that extracellular hemin may particularly affect cardiac function by modulating the electrical excitability of the heart.

Materials and methods

Cell culture and transfection

The coding sequence of human $Na_V1.5$ (*SCN5A*, Acc. no. Q14524) was expressed in HEK293T cells as described earlier (Chen and Heinemann 2001). Further variants used: $hNa_V1.2$ (NM001040143), $rNa_V1.2$ (P04775), $hNa_V1.4$ (AAO83647), $hNa_V1.7$ (NP002968), $hNa_V1.8c4$ (based on Q9Y5Y9.2), the latter being $hNa_V1.8$ with the C-terminal domain from $rNa_V1.4$ (P13390). All channel sequences were inserted into plasmids with CMV promoter.

For constructing domain-wise chimeras between $hNa_V1.5$ and $rNa_V1.2$, we introduced restriction sites into the sequence of $hNa_V1.5$ at the domain boundaries: MluI – domain I – BsiWI – domain II – NheI – domain III – ClaI – domain IX – XbaI. This construct, subcloned into a pcDNA3.1 (–) vector, was termed "5555". These select restriction sites were then used for cut-and-paste replacement of single domains by $rNa_V1.2$ domains, extracted from $rNa_V1.4$/$rNa_V1.2$ domain chimeras produced earlier (Zorn et al. 2006). The single-domain chimeras "2555" and "5552" did not yield sufficiently large currents. The combination "2552" did not express very well either but resulted in maximal current amplitudes of about 1 nA. Point mutations were introduced with PCR-based strategy followed by DNA sequencing.

Cells were transfected with the channel-coding plasmids using ROTI®Fect (Carl Roth, Karlsruhe, Germany). Visualization of transfected cells was achieved by coexpressing green fluorescent protein (GFP). The approximate concentration of GFP-coding DNA for transfection was 0.09 µg/mL; the concentration of the channel-coding DNA was adjusted according to the functional expression level (0.14–0.45 µg/mL).

Electrophysiological recording

Voltage-gated Na_V currents were measured in the whole-cell configuration of the patch-clamp method using an EPC10 amplifier and

PatchMaster data acquisition software (HEKA Elektronik, Lambrecht, Germany). Pipettes were fabricated from borosilicate glass with filament, tips coated with dental wax and fire-polished to yield resistances between 0.8 and 1.5 MΩ. Current data were typically sampled at a rate of 50 kHz with a 10-kHz low-pass antialiasing filter. Only cells with series resistance below 3 MΩ were accepted; the series resistance was corrected electronically up to 75%. Leak and capacitive currents were subtracted using a p/6 correction protocol. The junction potential of about −5 mV was not corrected for. For display and analysis purposes, current traces were further filtered with a Gaussian characteristic with a cutoff frequency of 4 kHz. Holding membrane voltage was −120 mV; before test pulses, the membrane was hyperpolarized to −140 mV for 50 ms to ensure complete recovery from inactivation. Data acquisition started after >10 min of equilibration of the cell at −120 mV in the whole-cell configuration. Agar bridges (1 M KCl, 1.5% agarose) were used for grounding the bath chamber.

All recordings were obtained at room temperature (20–23 °C). Hemin stock solution (1 mM) was made in 30 mM NaOH by rigorous vortexing (5 min) in the dark, either used immediately or aliquoted and stored at −20 °C. PpIX and dimethylhemin were dissolved in DMSO (1 mM), aliquoted and stored at −20 °C. For comparison (Figure 2), hemin stock solutions were also prepared in DMSO. On the day of experiments, stock solutions were kept on ice for up to 4 h. 1 mL predilution at a concentration to reach the desired final concentration was prepared immediately before application to the bath chamber (typically 2 or 4 mL); bath solutions were then mixed by pipetting.

Pipette solution composed of (in mM): 105 CsF, 35 NaCl, 10 ethylene glycol tetraacetic acid (EGTA), 10 4-(2-hydroxyethyl)-1-piperazineethanesulfonic acid (HEPES), pH was adjusted to 7.4 with CsOH. Bath solution: 146 NaCl, 2 $CaCl_2$, 2 $MgCl_2$, 4 KCl, 10 HEPES, pH 7.4 with NaOH.

Current-voltage relationships. Currents were elicited with depolarizing steps from −100 to 60 mV in steps of 10 mV. The resulting peak currents $I(V)$ were fit assuming a linear single-channel characteristic and $m = 3$ independent activation gates according to Hodgkin and Huxley:

$$I(V) = \Gamma\ (V - E_{rev})\left(1 + e^{-(V-V_m)/k_m}\right)^{-3} \quad (1)$$

with the total conductance Γ, the reversal potential E_{rev}, the half-maximal voltage of gate activation V_m, and the slope factor k_m characterizing the voltage dependence.

Voltage dependence of fast inactivation. Voltage dependence of fast inactivation was measured with a two-pulse protocol with depolarizations to −20 mV, separated by 920 ms intervals at variable voltage, V. The normalized peak currents were fit with a Boltzmann-type function,

$$\frac{I(V)}{I(-150mV)} = h_{max} - (h_{max} - h_{min})\left(1 + e^{-(V-V_h)/k_h}\right)^{-1} \quad (2)$$

yielding the half-maximal voltage of inactivation V_h and the slope factor k_h characterizing the voltage dependence; h_{min} and h_{max} denote the minimal and maximal channel availability relative to −150 mV, respectively.

Assessment of state or use dependence. The hemin impact on Na_V-mediated currents was analyzed with trains of depolarizing pulses (5 ms to −10 mV) applied at various frequencies. Furthermore, the amount of current inhibition was measured depending on prepulses that varied in duration and voltage. Respective pulse protocols are depicted in Figure 4 and Supplementary Figures 4 and 5.

Nonstationary noise analysis. Unitary single-channel conductance and the number of available channels per cell were estimated with nonstationary noise analysis as described earlier (Steffan and Heinemann 1997). In brief, 250 consecutive current data sweeps were recorded at an interval of 1.5 s, with each sweep containing pulses to −50, −30, and −10 mV as well as intercalating leak pulses to −90 mV. The resulting pairwise ensemble variance $\sigma(V)^2$ as a function of the leak-corrected mean current $I(V)$ at the three voltages were simultaneously fit according to (Heinemann and Leipold 2011):

$$\sigma(V)^2 = \sigma_b(V)^2 + \frac{iI - I^2}{N} \quad (3)$$

with the background variance σ_b^2, the single-channel current amplitude i, and the number of channels N, yielding 3 $i(V)$ values, together with the vanishing current at the reversal potential ($i(E_{rev}) = 0$), subsequently fit to a linear function for the control and in the presence of hemin:

$$i(V) = \gamma\ (V - E_{rev}) \quad (4)$$

thus, yielding an estimate of the single-channel conductance γ.

Chemicals

Hemin and protoporphyrin-IX as well as chemicals for preparing buffer solutions were purchased from Sigma/Aldrich.

Synthesis of dimethylhemin

Hemin was purchased from abcr GmbH (Karlsruhe, Germany). All other chemicals were purchased from Fisher Scientific and used without further purification. The reaction was performed under an atmosphere of argon using flame dried glassware. All flasks were equipped with rubber septa and reactants were handled using standard Schlenk techniques. Mass spectrometry was performed by using a Thermo Fisher Scientific LTQ Orbitrap XL (Ionization: Electron Spray Ionization, ESI).

To a stirring solution of hemin (0.10 g, 0.15 mmol, 1.00 eq.) in dry dimethylformamide (10 mL), sodium carbonate (0.24 g, 2.30 mmol, 15.0 eq.) and iodomethane (0.03 mL, 0.46 mmol, 3.00 eq.) were added successively before stirring overnight. Afterwards, the reaction mixture was filtered over a plug of Celite© and washed with dichloromethane (50 mL). The solvent was removed *in vacuo* and the residue was purified by normal phase flash chromatography on silica gel (ethyl acetate:methanol 24:1 + 2% acetic acid). Subsequent purification of the collected compound by reverse phase chromatography (C-18, acetonitrile:H_2O 4:1 to 19:1 +2% acetic acid) gave dimethylhemin (15.8 mg, 0.02 mmol, 15%) as a dark solid. HRMS (ESI(+), 6.0 eV): calculated. For $[M-Cl]^+$: 644.2081, found: 644.2084.

Electrostatic surface potentials

Electrostatic potential maps of heme, hemin, protoporphyrin IX, and dimethylhemin were calculated according to the Hartree–Fock formulation using GaussView 5.5/Gaussian 09. Where appropriate, each carboxylate group was assumed to be resonance stabilized and bear one negative charge. The structures were optimized and the electrostatic energies calculated with the 3-21G basis set and water solvation.

Data analysis

Data were analyzed with FitMaster (HEKA Elektronik), FITMASTER NEXT (Multi Channel Systems MCS GmbH, Reutlingen, Germany), and IgorPro 8 (WaveMetrics, Lake Oswego, OR, USA) software. Averaged data are presented with sem values.

The concentration dependence of hemin-induced current inhibition was described as follows,

$$\frac{I}{I_{\mathrm{Ctrl}}} = \frac{1}{1 + (c/IC_{50})^{n_{\mathrm{H}}}} \tag{5}$$

with the hemin concentration c, the half-maximal inhibitory constant IC_{50}, and the Hill coefficient n_{H}.

Acknowledgments: We thank Prof. Enrico Leipold (University of Lübeck, Germany) for constructing $hNa_V1.8c4$.

Author contributions: G.G.: study design, molecular biology of expression constructs, electrophysiological recordings, data analysis; M.J.: electrophysiological recordings, data analysis; P.T., D.M.: synthesis of dimethylhemin; R.S.: molecular biology of expression constructs; T.H.: structural modeling, data review, writing; S.H.H.: study design, data analysis, writing. All authors contributed to the editing of the manuscript.

Research funding: Support by the German Research Foundation (DFG, SHH: HE2993/18-1) and the National Institutes of Health (NIH, TH: GM121375).

Conflict of interest statement: The authors declare no conflicts of interest regarding this article.

References

Burton, M.J., Kapetanaki, S.M., Chernova, T., Jamieson, A.G., Dorlet, P., Santolini, J., Moody, P.C., Mitcheson, J.S., Davies, N.W., Schmid, R., et al. (2016). A heme-binding domain controls regulation of ATP-dependent potassium channels. Proc. Natl. Acad. Sci. USA 113: 3785–3790.

Burton, M.J., Cresser-Brown, J., Thomas, M., Portolano, N., Basran, J., Freeman, S.L., Kwon, H., Bottrill, A.R., Llansola-Portoles, M.J., Pascal, A.A., et al. (2020). Discovery of a heme-binding domain in a neuronal voltage-gated potassium channel. J. Biol. Chem. 295: 13277–13286.

Cader, A., Singh, S.M., and Zia, M.I. (2018). Brugada syndrome unmasked by malaria-induced fever. J. Cardiol. Cases 18: 136–137.

Chen, H. and Heinemann, S.H. (2001). Interaction of scorpion α-toxins with cardiac sodium channels: binding properties and enhancement of slow inactivation. J. Gen. Physiol. 117: 505–518.

Coburger, I., Yang, K., Bernert, A., Wiesel, E., Sahoo, N., Swain, S.M., Hoshi, T., Schönherr, R., and Heinemann, S.H. (2020). Impact of intracellular hemin on N-type inactivation of voltage-gated K^+ channels. Pflüger's Arch. 472: 551–560.

Crespo, E.M., Bhadra, K., and Lobel, R. (2009). Brugada syndrome unmasked by a mosquito. J. Hosp. Med. 4: E20–E22.

Daimi, H., Lozano-Velasco, E., Aranega, A., and Franco, D. (2022). Genomic and non-genomic regulatory mechanisms of the cardiac sodium channel in cardiac arrhythmias. Int. J. Mol. Sci. 23: 1381.

De Lera Ruiz, M. and Kraus, R.L. (2015). Voltage-gated sodium channels: structure, function, pharmacology, and clinical indications. J. Med. Chem. 58: 7093–7118.

Hanna, D.A., Harvey, R.M., Martinez-Guzman, O., Yuan, X., Chandrasekharan, B., Raju, G., Outten, F.W., Hamza, I., and Reddi, A.R. (2016). Heme dynamics and trafficking factors revealed by genetically encoded fluorescent heme sensors. Proc. Natl. Acad. Sci. USA 113: 7539–7544.

Heinemann, S.H. and Leipold, E. (2007). Conotoxins of the O-superfamily affecting voltage-gated sodium channels. Cell. Mol. Life Sci. 64: 1329–1340.

Heinemann, S.H. and Leipold, E. (2011). Tools for studying peptide toxin modulation of voltage-gated sodium channels. In: SFET editions. Toxins and Ion Transfers, Giv-sur-Yvette, pp. 29–37. http://www.sfet.asso.fr.

Heinemann, S.H., Terlau, H., and Imoto, K. (1992a). Molecular basis for pharmacological differences between brain and cardiac sodium channels. Pflüger's Arch. 422: 90–92.

Heinemann, S.H., Terlau, H., Stühmer, W., Imoto, K., and Numa, S. (1992b). Calcium channel characteristics conferred on the sodium channel by single mutations. Nature 356: 441–443.

Horrigan, F.T., Heinemann, S.H., and Hoshi, T. (2005). Heme regulates allosteric activation of the Slo1 BK channel. J. Gen. Physiol. 126: 7–21.

Jentho, E., Ruiz-Moreno, C., Novakovic, B., Kourtzelis, I., Megchelenbrink, W.L., Martins, R., Chavakis, T., Soares, M.P., Kalafati, L., Guerra, J., et al. (2021). Trained innate immunity, long-lasting epigenetic modulation, and skewed myelopoiesis by heme. Proc. Natl. Acad. Sci. USA 118: e2102698118.

Körner, J., Albani, S., Eswaran, V.S.B., Roehl, A.B., Rossetti, G., and Lampert, A. (2022). Sodium channels and local anesthetics - old friends with new perspectives. Front. Pharmacol. 13: 837088.

Leipold, E., HanseL, A., Borges, A., and Heinemann, S.H. (2006). Subtype specificity of scorpion β-toxin Tz1 interaction with voltage-gated sodium channels is determined by the pore loop of domain 3. Mol. Pharmacol. 70: 340–347.

Leipold, E., Debie, H., Zorn, S., Borges, A., Olivera, B.M., Terlau, H., and Heinemann, S.H. (2007). μO conotoxins inhibit Na_V channels by interfering with their voltage sensors in domain-2. Channels 1: 253–262.

Leipold, E., Borges, A., and Heinemann, S.H. (2012). Scorpion β-toxin interference with Na_V channel voltage sensor gives rise to excitatory and depressant modes. J. Gen. Physiol. 139: 305–319.

Li, K.H.C., Lee, S., Yin, C., Liu, T., Ngarmukos, T., Conte, G., Yan, G.X., Sy, R.W., Letsas, K.P., and Tse, G. (2020). Brugada syndrome: a comprehensive review of pathophysiological mechanisms and risk stratification strategies. Int. J. Cardiol. Heart Vasc. 26: 100468.

Li, Z., Jin, X., Wu, T., Huang, G., Wu, K., Lei, J., Pan, X., and Yan, N. (2021). Structural basis for pore blockade of the human cardiac sodium channel $Na_V1.5$ by the antiarrhythmic drug quinidine. Angew. Chem. Int. Ed. 60: 11474–11480.

Meggiolaro, M., Zorzi, A., Maghawry, M.E., Peruzza, F., Migliore, F., and Pittoni, G.M. (2013). Brugada ECG disclosed by acute malaria: is it all about fever and propofol? J. Clin. Anesth. 25: 483–487.

Ogawa, K., Sun, J., Taketani, S., Nakajima, O., Nishitani, C., Sassa, S., Hayashi, N., Yamamoto, M., Shibahara, S., Fujita, H., et al. (2001). Heme mediates derepression of Maf recognition element through direct binding to transcription repressor Bach1. EMBO J. 20: 2835–2843.

Ponka, P. (1999). Cell biology of heme. Am. J. Med. Sci. 318: 241–256.

Roumenina, L.T., Rayes, J., Lacroix-Desmazes, S., and Dimitrov, J.D. (2016). Heme: modulator of plasma systems in hemolytic diseases. Trends Mol. Med. 22: 200–213.

Sahoo, N., Goradia, N., Ohlenschläger, O., Schönherr, R., Friedrich, M., Plass, W., Kappl, R., Hoshi, T., and Heinemann, S.H. (2013). Heme impairs the ball-and-chain inactivation of potassium channels. Proc. Natl. Acad. Sci. USA 110: E4036–E4044.

Sahoo, N., Yang, K., Coburger, I., Bernert, A., Swain, S.M., Gessner, G., Kappl, R., Kühl, T., Imhof, D., Hoshi, T., et al. (2022). Intracellular hemin is a potent inhibitor of the voltage-gated potassium channel Kv10.1. Sci. Rep. 12: 14645.

Savio-Galimberti, E., Gollob, M.H., and Darbar, D. (2012). Voltage-gated sodium channels: biophysics, pharmacology, and related channelopathies. Front. Pharmacol. 3: 124.

Sawicki, K.T., Chang, H.C., and Ardehali, H. (2015). Role of heme in cardiovascular physiology and disease. J. Am. Heart Assoc. 4: e001138.

Soares, M.P. and Bozza, M.T. (2016). Red alert: labile heme is an alarmin. Curr. Opin. Immunol. 38: 94–100.

Steffan, R. and Heinemann, S.H. (1997). Error estimates for results of nonstationary noise analysis derived with linear least squares methods. J. Neurosci. Methods 78: 51–63.

Tang, X.D., Xu, R., Reynolds, M.F., Garcia, M.L., Heinemann, S.H., and Hoshi, T. (2003). Haem can bind to and inhibit mammalian calcium-dependent Slo1 BK channels. Nature 425: 531–535.

Tao, X., Lee, A., Limapichat, W., Dougherty, D.A., and Mackinnon, R. (2010). A gating charge transfer center in voltage sensors. Science 328: 67–73.

Terlau, H., Heinemann, S.H., Stühmer, W., Pusch, M., Conti, F., Imoto, K., and Numa, S. (1991). Mapping the site of block by tetrodotoxin and saxitoxin of sodium channel II. FEBS Lett. 293: 93–96.

Tsiftsoglou, A.S., Tsamadou, A.I., and Papadopoulou, L.C. (2006). Heme as key regulator of major mammalian cellular functions: molecular, cellular, and pharmacological aspects. Pharmacol. Ther. 111: 327–345.

Wang, S., Publicover, S., and Gu, Y. (2009). An oxygen-sensitive mechanism in regulation of epithelial sodium channel. Proc. Natl. Acad. Sci. USA 106: 2957–2962.

Wisedchaisri, G. and El-Din, T.M.G. (2022). Druggability of voltage-gated sodium channels - exploring old and new drug receptor sites. Front. Pharmacol. 13: 858348.

Wißbrock, A., Goradia, N.B., Kumar, A., Paul George, A.A., Kühl, T., Bellstedt, P., Ramachandran, R., Hoffmann, P., Galler, K., Popp, J., et al. (2019). Structural insights into heme binding to IL-36α proinflammatory cytokine. Sci. Rep. 9: 16893.

Zorn, S., Leipold, E., Hansel, A., Bulaj, G., Olivera, B.M., Terlau, H., and Heinemann, S.H. (2006). The μO-conotoxin MrVIA inhibits voltage-gated sodium channels by associating with domain-3. FEBS Lett. 580: 1360–1364.

Supplementary Material: The online version of this article offers supplementary material (https://doi.org/10.1515/hsz-2022-0194).